Minimally Invasive Characterization of Covalent Monolayer Sheets Using Tip-Enhanced Raman Spectroscopy

Lothar Opilik,[†] Payam Payamyar,[‡] Jacek Szczerbiński,[†] Andri P. Schütz,[‡] Marco Servalli,[‡] Tim Hungerland,[‡] A. Dieter Schlüter,[‡] and Renato Zenobi*[,†]

[†]Laboratory of Organic Chemistry, Department of Chemistry and Applied Biosciences, ETH Zurich, 8093 Zurich, Switzerland and [‡]Laboratory of Polymer Chemistry, Department of Materials, ETH Zurich, 8093 Zurich, Switzerland

ABSTRACT Synthetic covalent monolayer sheets and their subclass, two-dimensional polymers are of particular interest in materials science because of their special dimensionality which renders them very different from any bulk matter. However, structural analysis of such entities is rather challenging, and there is a clear need for additional analytical methods. The present study shows how tip-enhanced Raman spectroscopy (TERS) can be performed on monomer monolayers and the covalent sheets prepared from them by [4 + 4]-cycloaddition to explore rather complex structural and mechanistic issues. TERS is a surface analytical method that combines the high lateral resolution of scanning probe microscopy (SPM) with a greatly enhanced Raman scattering intensity. The high spatial resolution (<60 nm) and the significantly improved sensitivity (contrast factor of >4000) compared to confocal Raman microscopy provides new insights into the formation of this new and exciting material, namely significant consumption of the reactive units (anthracenes) and exclusion of the alternative [4 + 2]-cycloaddition. Moreover, due to the high lateral resolution, it was possible to find a first spectroscopic hint for step growth as the dominant mechanism in the formation of these novel monolayer sheets. In addition, TERS was used to get first insights into the phase behavior of a comonomer mixture.

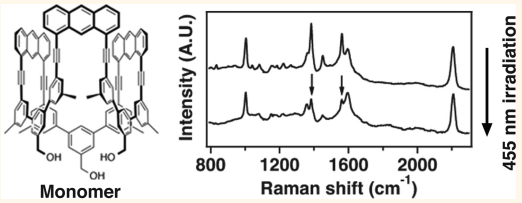

KEYWORDS: tip-enhanced Raman spectroscopy · TERS · 2D polymer · covalent monolayer · anthracene dimerization · nanoscale · imaging

Methods to obtain single sheets of layered inorganic materials (graphene, MoS_2, *etc.*) are, *e.g.*, micromechanical cleavage of the layered crystals[1] or chemical vapor deposition (CVD) on heated surfaces.[2] Even though thermolytic synthesis can result in large sheets,[3] it lacks the control of an organic synthesis approach, in particular in terms of functionality on the molecular level. Bottom-up synthesis of large one-repetition-unit thin sheets is challenging, and doing it in a controlled fashion would open up new possibilities to tailor their properties for different purposes, *e.g.*, as molecular sieves,[4] pressure sensors,[5] or 2D scaffolds for molecular ordering. The first experimental realizations were based on photochemical solid-state polymerization in preordered monomer crystals.[6,7] Because synthetic molecular sheets obtained after delamination from these crystals are not larger than a few micrometers, the synthesis of more extended covalent monolayers requires another approach. Recently, it was demonstrated that this can be accomplished by anthracene dimerization of compressed amphiphilic monomer units (see Figure 1) at an air–water interface.[8−10] The procedure can be carried out at room temperature and results in extended free-standing sheets. However, compared to the crystal approaches, suitable analytical methods to investigate the internal structure of these individual sheets are scarce. Powerful methods such as high-resolution transmission electron microscopy,[6] scanning probe microscopy,[6,11,12] X-ray diffraction,[6,11,12] solid-state nuclear magnetic resonance spectroscopy,[12] infrared spectroscopy,[7,11,12] and Raman spectroscopy[11] that can be used for crystal analysis are normally not suitable for the analysis of single molecular sheets. Some dedicated methods with single-sheet sensitivity exist, such as, *e.g.*, grazing incidence X-ray diffraction (GIXD) and infrared

* Address correspondence to zenobi@org.chem.ethz.ch.

Received for review January 28, 2015 and accepted March 24, 2015.

Published online March 24, 2015
10.1021/acsnano.5b00629

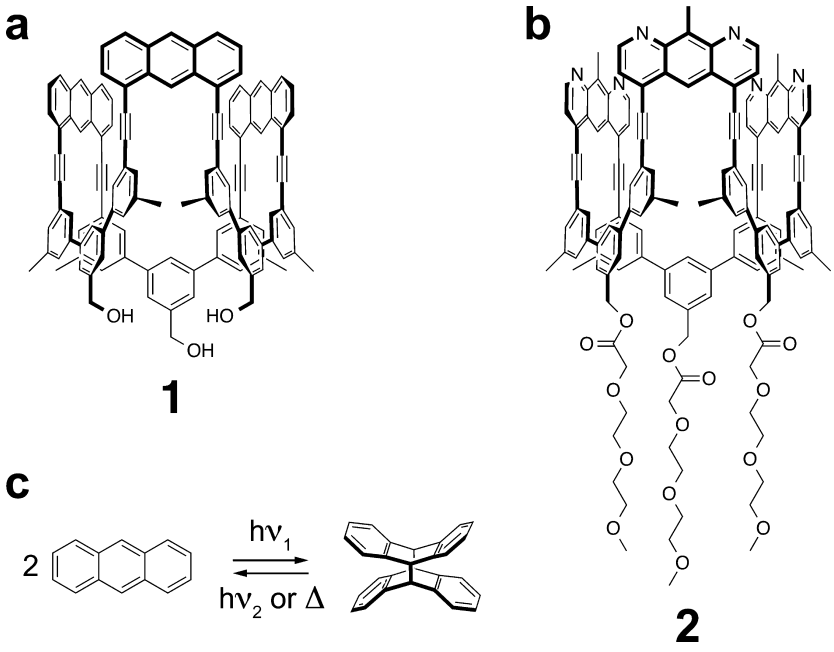

Figure 1. Amphiphilic and shape-persistent trifunctional monomer 1 (a) and monomer 2 (b). The photochemically reactive sites (anthracene moieties) are ideally positioned at an angle of 120° with respect to each other. The reaction scheme (c) shows the reversible photochemical anthracene dimerization (UV radiation with $\lambda_1 = c/\nu_1 > 300$ nm leads to dimerization, whereas UV radiation with $\lambda_2 = c/\nu_2 < 300$ nm leads to photodissociation).[20,21]

reflection–absorption (IRRA) spectroscopy;[13−15] however, these methods only provide limited lateral information. Electron microscopy and scanning probe microscopy are powerful methods to visualize structures that are far beyond the resolving power of an optical microscope. However, these methods do not give much information on the chemical composition. Moreover, the molecularly thin organic sheets are particularly sensitive to electron beam damage, restricting the acquisition of high-resolution transmission electron microscopy images. Confocal Raman spectroscopy can give detailed spectroscopic information with a lateral resolution down to approximately 200 nm at optical frequencies. Unfortunately, the typically low Raman cross-sections of most materials require strong laser irradiation and/or very long measurement times, which in the cases of molecularly thin sheets makes it almost impossible to obtain a spectrum at all. Enhancement of the Raman scattered light by metallic nanostructures (as in surface enhanced Raman spectroscopy, SERS) solves this issue. Our implementation (TERS) utilizes a scanning tunnelling microscopy (STM) tip as the enhancing nanostructure. This approach combines the enhancement with a greatly increased lateral resolution below the optical diffraction limit.[16,17] This gives the possibility of obtaining Raman spectra from very few or even single molecules[18] and to localize nanometer sized structural differences (*e.g.*, defects in single-layer graphene) with high precision.[19]

In the present study, TERS was used to probe the internal structure of novel covalent monomolecular sheets produced at the air–water interface by photoinduced anthracene dimerization between trifunctional monomers (see Figure 1). High-quality vibrational spectra from single/few layers of synthetic covalent monomolecular sheets are obtained. The spectra indicate that a significant fraction of the anthracene is consumed and potential side reactions can be excluded (*e.g.*, [4 + 2] cycloaddition between anthracene and alkyne). The spatial information from the TERS imaging experiments indicates that the remaining Raman intensity from unreacted anthracenes cannot be attributed to islands of unreacted monomers but is more or less homogeneously distributed (down to a lateral resolution of approximately 100 nm). Moreover, a first attempt was made to investigate mixed monolayers in two dimensions by this method.

RESULTS AND DISCUSSION

In order to evaluate the expected changes in the vibrational fingerprint spectrum upon polymerization, density functional theory (DFT) calculations of two model compounds were carried out (see Figure 2). The obtained theoretical spectra are in good agreement with the experimental Raman spectra from similar model compounds shown recently by Kissel *et al.*[6] A strong Raman band close to 2200 cm^{-1} corresponding to the triple bond stretching vibrations is observed for both model compounds but is omitted for better visibility of the spectral range below 1800 cm^{-1}. Raman bands that could be used for clear spectroscopic differentiation are marked with dashed lines. It

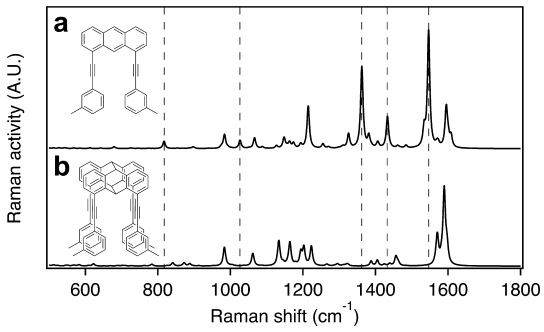

Figure 2. Theoretical Raman spectra of the indicated model compounds for the monomer molecule with intact anthracene moieties (a) and the covalent monolayer with dimerized anthracene moieties (b).

is apparent that the two most prominent peaks in the Raman spectrum for the unreacted monomer model compound (Figure 2a) at 1362 and 1546 cm^{-1} can be assigned to anthracene C═C stretching vibrations, whereas these modes are absent in the spectrum of the dimer model compound. In addition, the other indicated modes at 817, 1027, and 1433 cm^{-1} are dominated by anthracene vibrations. All these modes are clearly absent in the Raman spectrum of the dimer model (Figure 2b) and are therefore expected to disappear upon polymerization.

The differential interference contrast (DIC) microscopy image in Figure 3 shows the typical surface coverage of the covalent monolayer on gold after 3-fold deposition (see the Methods). It is possible to discern the covalent monolayers because of the clear contrast at the edges. The surface coverage is fairly high, and large sheets with a size in the range of a few hundred micrometers are observed. Few areas with a slightly darker appearance most likely indicate multilayers. Similar surface coverages were observed in the case of unreacted monomer layer deposition.

Confocal Raman spectra from single/few layers of the monomer on 300 nm SiO_2/Si substrates before and after irradiation only exhibit weak spectral features, even for an acquisition time of 30 min at 1.7 mW using 632.8 nm excitation, which does not allow any spectroscopic differentiation of the sheets before and after reaction because anthracene vibrational modes are almost completely missing in both cases (see Figure S1, Supporting Information). However, with a freshly prepared sharp silver tip in close proximity to the sample surface (maintained by STM feedback), Raman spectra exhibiting the characteristic peaks (including anthracene vibrational modes) were observed with a much lower laser power (30 μW) and a collection time of only 3 s. Figure 4 shows a typical tip-enhanced Raman spectrum from a nonirradiated monomer monolayer obtained after 3-fold deposition on gold. Direct comparison of the intensity of the triple-bond stretching vibration in a representative tip-enhanced Raman and a confocal Raman spectrum taking the

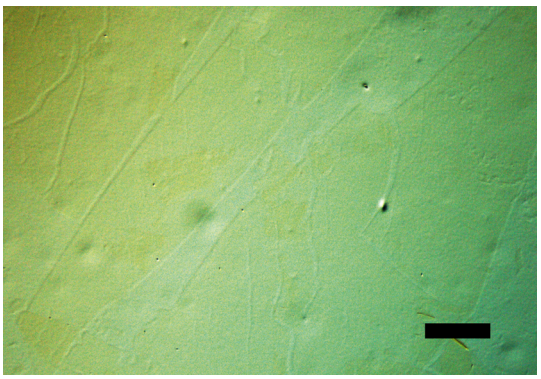

Figure 3. Differential interference contrast microscopy image of a covalent monolayer sheet after 3-fold deposition on a gold substrate. Individual layers can be recognized due to the clear contrast at the edges. The scale bar indicates 100 μm.

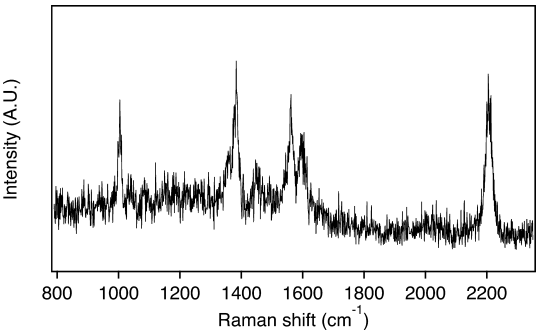

Figure 4. Tip-enhanced Raman spectrum from the monomer layer on gold (3-fold deposition). The observed spectral features correspond well to the theoretical spectra predicted by DFT calculations (see Figure 2).

different laser powers and acquisition times into account gives a contrast factor of >4000.

By scanning the tip across extended areas of the sample surface, spectroscopic images of the transferred monomer layers can be obtained. Figure 5a shows the sum of 1024 spectra from a 16 μm × 16 μm TERS map performed on a nonirradiated monomer layer on gold. The spectrum shows a high resemblance with the theoretical Raman spectrum (see Figure 2). The high abundance of the peaks at 1383 and 1562 cm^{-1} corresponding to anthracene vibrations indicate that the tightly packed monomers carry intact anthracene moieties.

This result is in conflict with the results of the above-mentioned confocal Raman measurements, where the anthracene modes were hardly observable. The reason could be that the high incident power and long acquisition time required to obtain the confocal Raman spectra alters the sample. It could, for example, be that despite the fact that the excitation wavelength of 632.8 nm is far away from the absorption band of the monomer,[8] the high energy flux leads to an anthracene dimerization or possible side reactions (*e.g.*, reaction with dioxygen[22]). This finding is a clear indication that TERS is a less invasive analytical method for

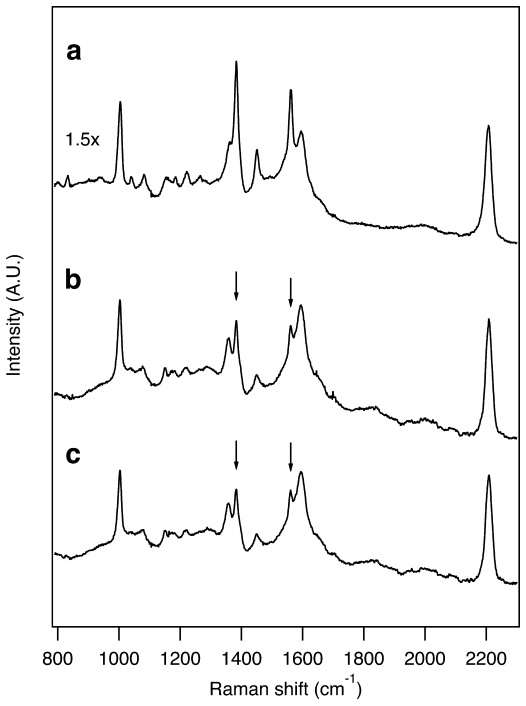

Figure 5. Accumulated spectrum from a TERS map of a nonirradiated 3-fold deposited monomer layer on gold (a) and accumulated spectra from two TERS maps of a 3-fold deposited monomer layer after irradiation with a 455 nm LED for 18 h (b, c). The arrows indicate the decrease in relative intensity of the most abundant anthracene vibrational modes. All maps have a size of 32 × 32 pixels and were performed on 16 μm × 16 μm and 20 μm × 20 μm areas, respectively. The spectra are offset for better visibility, and spectrum (a) was scaled in intensity with a factor of 1.5 for better comparability.

investigation of covalent monolayers than confocal Raman microscopy. In other words, TERS does not alter the specimen as much as Raman microscopy does, and consequently allows to probe these delicate molecule layers in a state close to native. Various examples where the applied analytical technique can cause changes in the investigated sample are known.[23,24] Moreover, the peaks at 1004 cm^{-1} (benzene ring breathing mode) and 2207 cm^{-1} (triple bond stretching) indicate integrity of the transferred molecules.

Dimerization of neighboring molecules was induced by irradiation of a packed monomer monolayer with a 455 nm LED for 18 h directly on the Langmuir trough. This was followed by transfer to a gold substrate (see Figure 3). Raman imaging experiments on the sheets were performed the same way as for the unreacted monomer layers. The accumulated tip-enhanced Raman spectra (1024 individual spectra) from two different sample positions are shown in Figure 5b,c. A significant decrease in relative peak intensity for the characteristic anthracene bands at 1383 and 1562 cm^{-1} was observed (indicated with arrows in Figure 5). Additional changes include a decrease in relative peak intensity for the anthracene ring breathing mode at 833 cm^{-1}, the anthracene C−H scissoring mode at 1040 cm^{-1}, and the anthracene C−H rocking/C=C stretching vibration at 1450 cm^{-1}. These observations are in agreement with the expected changes highlighted in the calculated spectra (see Figure 2). The residual intensity for the anthracene vibrational modes indicates the presence of unreacted anthracene units within the formed sheets. Payamyar *et al.* recently observed complete disappearance of the red-shifted anthracene fluorescence after 2 h irradiation at λ = 373 nm based on *in situ* measurements at the air/water interface.[8] This discrepancy is most likely caused by the 2 orders of magnitude lower photon flux used in the present study resulting in an incomplete photochemical reaction even after 18 h irradiation. A well-known competitive reaction to anthracene dimerization is its oxidation through a [4 + 2] photoaddition. With the evidence that netpoint formation even occurred at high oxygen levels, Payamyar *et al.* showed that the oxidation product is not competitive with photodimerization.[8] Spectroscopic analysis would in principle allow a more quantitative evaluation of the dimer to oxide ratio. For TERS, a spectral signature of the oxidation product is expected at approximately 1650 cm^{-1} (C=O stretching vibration) and was not observed. However, it could be obstructed by the broad peak at 1595 cm^{-1} (benzene C=C stretching vibration). The possible competing light-induced [4 + 2] cycloaddition between anthracene and the alkyne functionality[6] can be excluded because the relative triple bond peak intensity is essentially unchanged after irradiation. The preference for the [4 + 4] cycloaddition is most likely of steric nature and caused by the close stacking of the anthracene moieties on the Langmuir trough (supported by the observation of excimer fluorescence[8]). No vibrational modes related to the newly formed bonds between the two anthracene moieties (expected at 892 and 841 cm^{-1}) were observed. One reason could be that the sheets formed are amorphous, which would imply that no discrete vibrational mode for the newly formed C−C bonds would be expected. Another reason could be that the vibrational modes of these newly formed bonds oriented parallel to the sample surface are not as effectively enhanced as modes that are oriented perpendicular to the surface and thus more prominent in the spectra. A similar finding was recently reported on single-layer graphene imaged with the same TERS configuration.[19]

In a next step, we used the spatial information encoded in TERS maps. To prove that TERS imaging on the covalent monolayers actually probes the local chemical composition, an imaging experiment was conducted at the edge of one of the covalent sheets. A Raman intensity image (32 pixels × 32 pixels, 4 μm × 4 μm) evaluated for the triple-bond stretching vibration is shown in Figure 6. The distance between two subsequent points is 129 nm. The immediate drop in

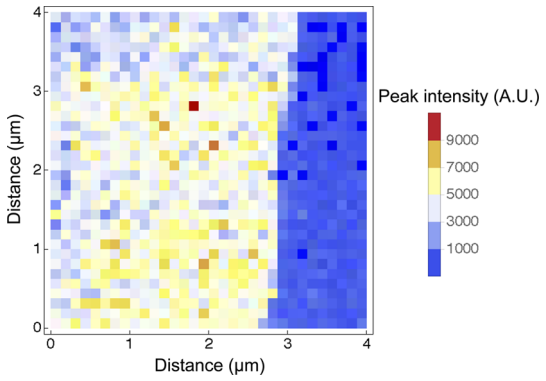

Figure 6. Raman intensity image of the triple bond stretching vibration across the edge of a covalent sheet on gold.

Raman intensity at the edge (from one point to the next) indicates that the actual lateral resolution is below the optical diffraction limit at the used wavelength (a spectroscopic image across the film edge with an even smaller step size of 60 nm is shown in Figure S2 in the Supporting Information).

In order to investigate the spatial distribution of the residual anthracene moieties indicated by the residual peak intensities at 1383 and 1562 cm^{-1} in the accumulated spectrum in Figure 5b, the ratio of the two neighboring peaks at 1562 and 1595 cm^{-1} was evaluated at every position of the map, only taking into account peaks with an intensity above the three times noise criterion. A well-defined Gaussian distribution of the peak ratio of 0.75 $\pm$ 0.18 was found (for the 18 h irradiated sample), which is significantly below the ratio of 1.29 $\pm$ 0.40 found for the nonirradiated monomer monolayer (see Figures S3 and S5 in the Supporting Information). This finding suggests a homogeneous consumption of anthracene within the sheet. To look into this in more detail, a TERS map with a smaller step size (103 nm) was performed on a layer (one-time transfer) that had only been irradiated for 20 min at 455 nm. The observed peak ratio distribution was again found to be well-approximated by a Gaussian function with a value of 0.94 $\pm$ 0.24 (see Figure S4 in the Supporting Information). The fact that the anthracene consumption is reflected in well-defined peak-ratio distributions at all investigated stages of the reaction is an indication that the formation of the covalent sheets probably happens with a step-growth mechanism. In the case of a chain-growth mechanism, a less defined intensity distribution would be expected (if the lateral resolution is high enough) with more values at the initial peak ratio of the unreacted monomer. However, a reliable examination would require spectroscopic analysis down to the single molecule level which has not been possible so far.

An example where the spatial information provided by TERS imaging is of particular value is the spectroscopic analysis of mixed monomer monolayers. When considering a binary mixture of monomers 1 and 2

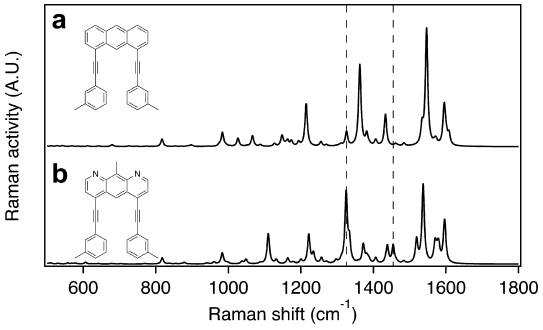

Figure 7. Theoretical Raman spectra of model compounds for the two premixed monomers with an anthracene (a) and an 1,8-diazaanthracene (b) moiety, respectively.

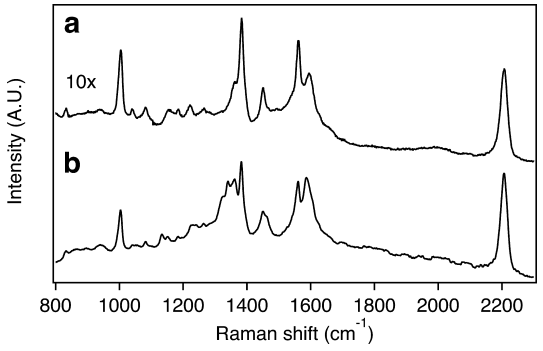

Figure 8. Accumulated spectrum from a TERS map with 32 $\times$ 32 pixels on a 20 μm $\times$ 20 μm area of a 1:1 mixed monolayer of monomers 1 and 2 (b) compared to the accumulated spectrum of a pure 3-fold deposited monomer 1 layer (a). The spectra are offset for better visibility, and spectrum a was scaled in intensity with a factor of 10 for better comparability.

(see Figure 1), the phase behavior on the Langmuir trough will predetermine the structure of the resulting two-dimensional copolymer.[10] We made a first attempt to study a binary mixture of monomers 1 and 2 in a molar ratio of 1:1 by performing a TERS imaging experiment on a premixed monomer layer prepared on a Langmuir trough and transferred to a gold substrate by one-time transfer.

Figure 7 shows the predicted Raman spectra of the corresponding model compounds. Spectroscopic contrast is given by a shift of one of the anthracene C=C (respectively C=N) stretching vibrations to a lower wavenumber (namely 1325 cm^{-1}) because of strong involvement of the nitrogen atoms. Differentiation is also possible based on the additional peak at 1455 cm^{-1}, which corresponds to a vibrational mode with strong involvement of the additional methyl group at the 9-position of anthracene.

TERS imaging on a 1:1 mixed monolayer of monomers 1 and 2 was performed on a 20 μm $\times$ 20 μm area (32 $\times$ 32 pixels), and the resulting accumulated spectrum is shown in Figure 8b. Direct comparison to the accumulated spectrum from the pure monomer 1 layer (Figure 8a) indicates a significant decrease in intensity of the two anthracene C=C stretching modes. Moreover,

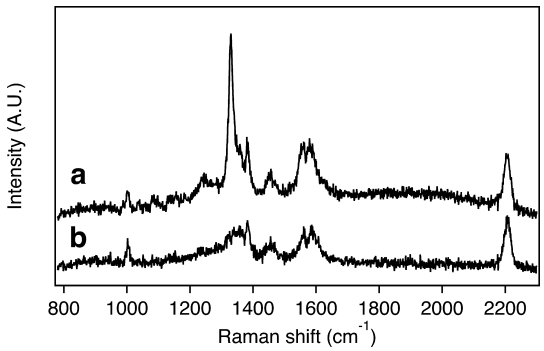

Figure 9. Tip-enhanced Raman spectra extracted from the map underlying the accumulated spectrum in Figure 8. Few spectra show a particularly strong peak at 1330 cm^{-1} (a), whereas in the other spectra (b), this peak is only of moderate intensity. The spectra are offset for better visibility.

additional modes are observed at 1330, 1341, and 1462 cm^{-1}, which can be assigned to monomer 2 vibrations (see Figure 7).

It is again possible to perform a spatial analysis similar to the one applied for the pure monomer layers. The intensity ratio of the peaks at 1562 and 1595 cm^{-1} shows a well-defined distribution of 0.83 $\pm$ 0.11 (see Figure S6 in the Supporting Information). The significantly lower ratio compared to the pure layer of monomer 1 can be explained by the fact that the two monomers appear to be homogeneously mixed on the sample surface (within the resolution limit). In the case of a heterogeneous distribution, ratios as observed for the pure monomer 1 layers would appear more frequently. Interestingly, some spectra exhibit a particularly intense peak at 1330 cm^{-1}, which can be attributed to a characteristic vibrational mode of monomer 2 (see above) (Figure 9). However, these spectra did not show any significant decrease in band intensity for the anthracene modes at 1383 and 1562 cm^{-1}. The particularly high peak intensity of the 1,8-diazaanthracene C=C/C=N stretching vibration at 1330 cm^{-1} could be a result of a direct interaction of the nitrogen lone pair with silver atoms of the tip. This additional enhancement effect is known as chemical enhancement in the surface-enhanced Raman spectroscopy literature.[25] Work by Hayazawa *et al.* even reported splitting of the ring-breathing mode of adenine crystals caused by direct interaction between the atoms of a silver tip and the nitrogen atoms.[26]

CONCLUSIONS

In the present study, TERS was used for the first time to obtain high signal-to-noise Raman spectra from single/few layers of a synthetic covalent sheet. The orders of magnitude higher sensitivity compared to confocal Raman microscopy allows to use acquisition times of a few seconds and laser powers in the low μW range, which significantly reduces invasiveness of the analytical method in the case of susceptible samples.

A clear intensity decrease of the characteristic anthracene vibrations indicates successful dimerization of neighboring monomers within compressed layers on the Langmuir trough. The potential side reaction of a [4 + 2] cycloaddition could be excluded on the basis of the rich spectroscopic information. The laterally resolved spectroscopic data shows a well-defined distribution of unreacted monomer units within a partially reacted layer based on individual spectra from <5000 monomers collected from sample positions separated by approximately 100 nm. No domains were found on the investigated length scale. Since the formation of covalent nanosheets would be favored in the case of a chain growth mechanism, this finding indicates that the polymerization in two dimensions probably happens with a step growth mechanism. However, a more reliable examination would require to push the lateral resolution further toward the single/few-molecule level. Moreover, a first attempt toward the high-resolution spectroscopic mapping of two-dimensional copolymers was made. The possibility to image the lateral molecular distribution with high resolution could allow to shine light on the processes involved in the formation of two-dimensional molecular films, especially in the case of copolymerization. The differentiation of gradient and random copolymers, for example, is only possible on the molecular or close to molecular level.[27] A possibility would also be to use the tip enhancement not as an analytical tool, but to produce nanoscale covalent sheets with a predefined shape. This could, for example, be realized by using plasmonic silver or aluminum tips with UV irradiation to locally induce anthracene dimerization.

METHODS

A Langmuir trough (Minitrough, KSV, Finland) was used to create monomer monolayers at the air–water interface (details can be found in Payamyar *et al.*[8,10]). A platinum Wilhelmy balance allowed us to monitor the surface pressure. In-plane polymerization was induced at a pressure of 20 mN/m by irradiating a circular area (Ø 1–2 cm) of the monolayer with a fiber-coupled 455 nm light emitting diode (300 mW, LEDMOD OEM, Omicron-Laserage Laserprodukte GmbH, Germany) for up to 18 h. Two different methods were used to transfer monomer monolayers and polymer sheets onto gold and 300 nm SiO_2/Si substrates at a surface pressure of 20 mN/m and a transfer speed of 1 mm/min. First, samples were produced by three consecutive vertical Langmuir–Blodgett transfers. The 3-fold deposition is done to increase the surface coverage because the film easily breaks apart. Second, substrates were pulled through the molecular film on the water surface at an angle of approximately 45°, which results in almost full surface coverage with one layer at most. Coverage of the substrate is typically checked using a reflected light DIC microscope (DM4000 M, Leica Microsystems). Flat gold substrates were prepared by a template-stripping method described in more detail elsewhere.[28,29]

TERS measurements were performed on a combined STM/Raman microscope (NTEGRA Spectra Upright, NT-MDT, Zelenograd, Russia) using a 632.8 nm HeNe laser for Raman excitation. The instrument is equipped with an electron multiplying charge-coupled device (EMCCD, Newton 971 UVB, Andor, Belfast, UK). Silver tips with typical radii of curvature of 40−120 nm were prepared by electrochemical etching of a silver wire (diameter 0.25 mm, 99.99% purity, Sigma-Aldrich). A 2:1 (v/v) mixture of methanol (p.a., Sigma-Aldrich) and perchloric acid (70%, VWR) was used as etchant. Tip-enhanced Raman spectra were collected after focusing the excitation laser on the apex of a silver tip in scanning tunnelling feedback (constant current mode) with the sample surface. Imaging was performed by moving the piezo sample stage in the *x*, *y*, and *z* directions while keeping the relative laser-to-tip position fixed. An acquisition time of 3 s was used for all shown spectra. A fairly low laser power of 30 μW on the sample stage was chosen in order to minimize photoinduced reactions/decomposition of the sample molecules.

Theoretical Raman activity spectra were calculated using Gaussian 09 (Gaussian, Wallingford, CT).[30] Optimization of the molecular structures was performed by means of density functional theory (DFT). The Becke, three-parameter Lee−Yang−Parr (B3LYP) exchange-correlation functional with the 6-311G(d) basis set was used for all atoms. The vibrational modes were assigned on the basis of visual inspection in GaussView 5. All calculated frequencies were scaled with a factor of 0.970.

Accumulated spectra from each map were fitted with a third-order polynomial baseline fit and with Lorentzians for the main peaks (up to 10 for the monomer mixtures) and for all other spectral features. The spatial maps shown are based on the peak area determined from fits to individual spectra with the constraints of fixed peak positions and full width at half maxima from the fit of the accumulated spectra. The peak heights were determined by means of an automatic peak finder based on Gaussian filtering of the spectra (Mathematica 10, Wolfram Research, Oxfordshire, UK) and an individual threshold for each spectrum (after baseline subtraction) corresponding to a three times noise criterion. The determined peak ratios with their uncertainties are calculated as mean $\pm$ 2 standard deviations from the spectra that fulfill the aforementioned criterion.

Conflict of Interest: The authors declare no competing financial interest.

Acknowledgment. We thank the HPC (High Performance Computing) Team at ETH Zurich, in particular S. Fux, for their support with the Brutus Cluster, which was used for some of the DFT calculations shown.

Supporting Information Available: Confocal Raman spectra, additional TERS images, and peak ratio histograms extracted from TERS images. This material is available free of charge *via* the Internet at http://pubs.acs.org/.

REFERENCES AND NOTES

1. Novoselov, K. S.; Jiang, D.; Schedin, F.; Booth, T. J.; Khotkevich, V. V.; Morozov, S. V.; Geim, A. K. Two-Dimensional Atomic Crystals. *Proc. Natl. Acad. Sci. U.S.A.* **2005**, *102*, 10451.
2. Reina, A.; Jia, X.; Ho, J.; Nezich, D.; Son, H.; Bulovic, V.; Dresselhaus, M. S.; Kong, J. Large Area, Few-Layer Graphene Films on Arbitrary Substrates by Chemical Vapor Deposition. *Nano Lett.* **2009**, *9*, 30–35.
3. Bae, S.; Kim, H.; Lee, Y.; Xu, X.; Park, J.-S.; Zheng, Y.; Balakrishnan, J.; Lei, T.; Kim, H. R.; Il Song, Y.; et al. Roll-to-Roll Production of 30-Inch Graphene Films for Transparent Electrodes. *Nat. Nanotechnol.* **2010**, *5*, 574–578.
4. Celebi, K.; Buchheim, J.; Wyss, R. M.; Droudian, A.; Gasser, P.; Shorubalko, I.; Kye, J.-I.; Lee, C.; Park, H. G. Ultimate Permeation Across Atomically Thin Porous Graphene. *Science* **2014**, *344*, 289–292.
5. Smith, A. D.; Vaziri, S.; Niklaus, F.; Fischer, A. C.; Sterner, M.; Delin, A.; Östling, M.; Lemme, M. C. Pressure Sensors Based on Suspended Graphene Membranes. *Solid-State Electron.* **2013**, *88*, 89–94.
6. Kissel, P.; Erni, R.; Schweizer, W. B.; Rossell, M. D.; King, B. T.; Bauer, T.; Götzinger, S.; Schlüter, A. D.; Sakamoto, J. A Two-Dimensional Polymer Prepared by Organic Synthesis. *Nat. Chem.* **2012**, *4*, 287–291.
7. Bhola, R.; Payamyar, P.; Murray, D. J.; Kumar, B.; Teator, A. J.; Schmidt, M. U.; Hammer, S. M.; Saha, A.; Sakamoto, J.; Schlüter, A. D.; et al. A Two-Dimensional Polymer from the Anthracene Dimer and Triptycene Motifs. *J. Am. Chem. Soc.* **2013**, *135*, 14134–14141.
8. Payamyar, P.; Kaja, K.; Ruiz-Vargas, C.; Stemmer, A.; Murray, D. J.; Johnson, C. J.; King, B. T.; Schiffmann, F.; VandeVondele, J.; Renn, A.; et al. Synthesis of a Covalent Monolayer Sheet by Photochemical Anthracene Dimerization at the Air/Water Interface and its Mechanical Characterization by AFM Indentation. *Adv. Mater.* **2014**, *26*, 2052–2058.
9. Chen, Y.; Li, M.; Payamyar, P.; Zheng, Z.; Sakamoto, J.; Schlüter, A. D. Room Temperature Synthesis of a Covalent Monolayer Sheet at Air/Water Interface Using a Shape-Persistent Photoreactive Amphiphilic Monomer. *ACS Macro Lett.* **2014**, *3*, 153–158.
10. Payamyar, P.; Servalli, M.; Hungerland, T.; Schütz, A. P.; Zheng, Z.; Borgschulte, A.; Schlüter, A. D. Approaching Two-Dimensional Copolymers: Photoirradiation of Anthracene- and Diaza-Anthracene-Bearing Monomers in Langmuir Monolayers. *Macromol. Rapid Commun.* **2015**, *36*, 151–158.
11. Kissel, P.; Murray, D. J.; Wulftange, W. J.; Catalano, V. J.; King, B. T. A Nanoporous Two-Dimensional Polymer by Single-Crystal-to-Single-Crystal Photopolymerization. *Nat. Chem.* **2014**, *6*, 774–778.
12. Kory, M. J.; Wörle, M.; Weber, T.; Payamyar, P.; van de Poll, S. W.; Dshemuchadse, J.; Trapp, N.; Schlüter, A. D. Gram-Scale Synthesis of Two-Dimensional Polymer Crystals and Their Structure Analysis by X-Ray Diffraction. *Nat. Chem.* **2014**, *6*, 779–784.
13. Kaganer, V. M.; Möhwald, H.; Dutta, P. Structure and Phase Transitions in Langmuir Monolayers. *Rev. Mod. Phys.* **1999**, *71*, 779–819.
14. Peng, J. B.; Barnes, G. T.; Gentle, I. R. The Structures of Langmuir-Blodgett Films of Fatty Acids and Their Salts. *Adv. Colloid Interface Sci.* **2001**, *91*, 163–219.
15. Schrettl, S.; Stefaniu, C.; Schwieger, C.; Pasche, G.; Oveisi, E.; Fontana, Y.; Morral, A. F. i.; Reguera, J.; Petraglia, R.; Corminboeuf, C.; et al. Functional Carbon Nanosheets Prepared from Hexayne Amphiphile Monolayers at Room Temperature. *Nat. Chem.* **2014**, *6*, 468–476.
16. Stadler, J.; Schmid, T.; Zenobi, R. Nanoscale Chemical Imaging Using Top-Illumination Tip-Enhanced Raman Spectroscopy. *Nano Lett.* **2010**, *10*, 4514–4520.
17. Anderson, N.; Hartschuh, A.; Cronin, S.; Novotny, L. Nanoscale Vibrational Analysis of Single-Walled Carbon Nanotubes. *J. Am. Chem. Soc.* **2005**, *127*, 2533–2537.
18. Zhang, R.; Zhang, Y.; Dong, Z. C.; Jiang, S.; Zhang, C.; Chen, L. G.; Zhang, L.; Liao, Y.; Aizpurua, J.; Luo, Y.; et al. Chemical Mapping of a Single Molecule by Plasmon-Enhanced Raman Scattering. *Nature* **2013**, *498*, 82–86.
19. Stadler, J.; Schmid, T.; Zenobi, R. Nanoscale Chemical Imaging of Single-Layer Graphene. *ACS Nano* **2011**, *5*, 8442–8448.
20. Bouas-Laurent, H.; Castellan, A.; Desvergne, J.-P.; Lapouyade, R. Photodimerization of Anthracenes in Fluid Solution: Structural Aspects. *Chem. Soc. Rev.* **2000**, *29*, 43–55.
21. Bouas-Laurent, H.; Castellan, A.; Desvergne, J.-P.; Lapouyade, R. Photodimerization of Anthracenes in Fluid Solutions: (Part 2) Mechanistic Aspects of the Photocycloaddition and of the Photochemical and Thermal Cleavage. *Chem. Soc. Rev.* **2001**, *30*, 248–263.
22. Fudickar, W.; Linker, T. Novel Anthracene Materials for Applications in Lithography and Reversible Photoswitching by Light and Air. *Langmuir* **2010**, *26*, 4421–4428.
23. Puppels, G. J.; Olminkhof, J. H. F.; Segers-Nolten, G. M. J.; Otto, C.; DeMul, F. F. M.; Greve, J. Laser Irradiation and

Raman Spectroscopy of Single Living Cells and Chromosomes: Sample Degradation Occurs With 514.5 nm But Not With 660 nm Laser Light. *Exp. Cell Res.* **1991**, *195*, 361–367.
24. Egerton, R. F.; Li, P.; Malac, M. Radiation Damage in the TEM and SEM. *Micron* **2004**, *35*, 399–409.
25. Campion, A.; Kambhampati, P. Surface-Enhanced Raman Scattering. *Chem. Soc. Rev.* **1998**, *27*, 241–250.
26. Hayazawa, N.; Watanabe, H.; Saito, Y.; Kawata, S. Towards Atomic Site-Selective Sensitivity in Tip-Enhanced Raman Spectroscopy. *J. Chem. Phys.* **2006**, *125*, 244706.
27. Sakamoto, J.; van Heijst, J.; Lukin, O.; Schlüter, A. D. Two-Dimensional Polymers: Just a Dream of Synthetic Chemists? *Angew. Chem., Int. Ed.* **2009**, *48*, 1030–1069.
28. Stadler, J.; Schmid, T.; Opilik, L.; Kuhn, P.; Dittrich, P. S.; Zenobi, R. Tip-Enhanced Raman Spectroscopic Imaging of Patterned Thiol Monolayers. *Beilstein J. Nanotechnol.* **2011**, *2*, 509–515.
29. Weiss, E. A.; Kaufman, G. K.; Kriebel, J. K.; Li, Z.; Schalek, R.; Whitesides, G. M. Si/SiO_2-Templated Formation of Ultraflat Metal Surfaces on Glass, Polymer, and Solder Supports: Their Use as Substrates for Self-Assembled Monolayers. *Langmuir* **2007**, *23*, 9686–9694.
30. Frisch, M. J.; Trucks, G. W.; Schlegel, H. B.; Scuseria, G. E.; Robb, M. A.; Cheeseman, J. R.; Scalmani, G.; Barone, V.; Mennucci, B.; Petersson, G. A.; Nakatsuji, H.; Caricato, M.; Li, X.; Hratchian, H. P.; Izmaylov, A. F.; Bloino, J.; Zheng, G.; Sonnenberg, J. L.; Hada, M.; Ehara, M.; Toyota, K.; Fukuda, R.; Hasegawa, J.; Ishida, M.; Nakajima, T.; Honda, Y.; Kitao, O.; Nakai, H.; Vreven, T.; Montgomery, J. A., Jr.; Peralta, J. E.; Ogliaro, F.; Bearpar, M.; Heyd, J.J.; Brothers, E.; Kudin, K. N.; Staroverov, V. N.; Kobayashi, R.; Normand, J.; Raghavachari, K.; Rendell, A.; Burant, J. C.; Iyengar, S. S.; Tomasi, J.; Cossi, M.; Rega, N.; Millam, J. M.; Klene, M.; Knox, J. E.; Cross, J. B.; Bakken, V.; Adamo, C.; Jaramillo, J.; Gomperts, R.; Stratmann, R. E.; Yazyev, O.; Austin, A. J.; Cammi, R.; Pomelli, C.; Ochterski, J. W.; Martin, R. L.; Morokuma, K.; Zakrzewski, V. G.; Voth, G. A.; Salvador, P.; Dannenberg, J. J.; Dapprich, S.; Daniels, A. D.; Farkas, Ö.; Foresman, J. B.; Ortiz, J. V.; Cioslowski, J.; Fox, D. J. *Gaussian 09, Revision D.01*, Gaussian, Inc.: Wallingford, CT, 2009.